Paramagnetic shimming for wide-range variable-field NMR.

AUTHOR(S):

Ichijo, Naoki; Takeda, Kazuyuki; Takegoshi, K

CITATION:

Ichijo, Naoki ...[et al]. Paramagnetic shimming for wide-range variable-field NMR.. Journal of magnetic resonance 2014, 246: 57-61

ISSUE DATE:

2014-07-12

URL:

http://hdl.handle.net/2433/189435

Paramagnetic shimming for wide-range variable-field NMR

Naoki Ichijo, Kazuyuki Takeda *, K. Takegoshi

Division of Chemistry, Graduate School of Science, Kyoto University, 606-8502 Kyoto, Japan

Abstract

We propose a new passive shimming strategy for variable-field NMR experiments, in which the magnetic field produced by paramagnetic shim pieces placed inside the magnet bore compensates the inhomogeneity of a variable-field magnet for a wide range of magnet currents. Paramagnetic shimming is demonstrated in ^{7}Li, ^{87}Rb, and ^{45}Sc NMR of a liquid solution sample in magnetic fields of 3.4, 4.0, and 5.4 T at a fixed carrier frequency of 56.0 MHz. Since both the main-field inhomogeneity and the paramagnetic magnetization are proportional to the main-magnet current, the resonance lines are equally narrowed by the improved field homogeneity with an identical configuration of the paramagnetic shim pieces. Paramagnetic shimming presented in this work opens the possibility of high-resolution variable-field NMR experiments.

Key words: shimming; passive shimming; paramagnetic shimming; variable-field superconducting magnet; NMR elemental analysis

* corresponding author
Email address: takezo@kuchem.kyoto-u.ac.jp (Kazuyuki Takeda).

1 Introduction

High-resolution nuclear magnetic resonance (NMR) and magnetic resonance imaging (MRI) experiments require a strong, stable, and homogeneous magnetic field over the sample volume. For typical superconducting magnets used widely nowadays, field homogeneity is not satisfactory, so that shimming is essential for high-resolution measurements. Shimming can be performed in two ways: *active* and *passive* shimming. Active or electric shimming is to employ shim coils producing various magnetic field profiles, and to adjust the currents flowing through them to ameliorate field homogeneity [1]. Such shim coils are often wound with superconducting wires and embedded in the cryostat of the superconducting magnet for coarse shimming. In high-resolution NMR, it is common to employ additional room shim coils inside the magnet bore for further improvement of the field homogeneity. The other way, passive shimming, is to place pieces of steel in such a way that the original field inhomogeneity is diminished [2]. Both the active and passive shimming schemes are well established and expected to work at a constant magnetic field.

However, operation of the magnet over a wide range of magnetic fields is also of interest in NMR spectroscopy. In NMR of condensed matter, resonance lines are too broad in many cases to be covered with the bandwidth of a tuned circuit. In such cases, experiments with varied magnetic fields are convenient, rather than fixed-field measurements. There, little attention has been paid to the field homogeneity, as the line-broadening effect is masked by the intrinsic linewidth. Nevertheless, shimming will also be important in the variable-field experiments. For example, in quantitative NMR elemental analysis that we recently reported [3], variable-field NMR measurement at a fixed carrier fre-

quency enabled us to access to various nuclear spin species with a common detection efficiency, leading to quantitative determination of the isotopes. Due to the insufficient homogeneity of the variable-field superconducting magnet used in that study, the spectral resolution was not high enough to reveal chemical information. Indeed, the variable-field superconducting magnets are widespread for use in various scientific research fields, but not in NMR for chemical analysis where the requirement for the homogeneity is so demanding. Thus, field correction of a number of existing systems which do not employ the superconducting shims is of interest.

In principle, both the electric and ferromagnetic shimming schemes are expected to work by changing the currents or configuration every time the magnetic field is altered. However, this would be quite formidable and not practical. What is required is a new shimming strategy that is convenient and works over a wide range of magnetic fields. In this work, we present one such. Our approach is categorized into passive shimming, in the sense that no electric current is applied. Instead of the ferromagnetic steel pieces, we employ pieces of *paramagnetic* material. So far, passive shimming with paramagnetic and diamagnetic materials has been reported [4,5], but only in the context of high-order local field correction in fixed-field MRI experiments. Here, we exploit one important property of the paramagnetic material; the magnetization and thereby the produced magnetic field are proportional to the main-field strength. It follows that, once field correction by paramagnetic shimming has been done for one given field strength, the identical shim configuration should also work at any other field strengths. This is in contrast to the ferromagnetic steel shim, in which the magnetization is saturated, so that one would have to modify the shim configuration whenever the field strength is altered.

Therefore, paramagnetic shimming proposed in this work would provide a convenient and effective way to high-resolution variable-field NMR studies. In the following, we demonstrate field correction using pieces of Dy_2O_3 in a cryogen-free superconducting magnet, examining NMR spectra of ^{7}Li, ^{87}Rb, and ^{45}Sc measured in magnetic fields of 3.4, 4.0, and 5.4 T at a fixed frequency of 56 MHz.

2 Strategy

The idea of passive shimming is to place a number of magnetic pieces so that the net magnetic field they produce cancels the original field inhomogeneity. In general, the problem of finding the right shim configuration is formulated as [6]

$$\mathbf{B}_{\mathrm{shim}} = \mathbf{A} \cdot \mathbf{M}. \tag{1}$$

Here, $\mathbf{B}_{\mathrm{shim}} = (B_{\mathrm{shim}}(\mathbf{r}_1), B_{\mathrm{shim}}(\mathbf{r}_2), \cdots, B_{\mathrm{shim}}(\mathbf{r}_n))$ is an n-dimensional vector with its elements being the z-components of the magnetic field at positions $\{\mathbf{r}_1, \mathbf{r}_2, \cdots, \mathbf{r}_n\}$ produced by the magnetization of the shim pieces $\mathbf{M} = (M(\mathbf{s}_1), M(\mathbf{s}_2), \cdots, M(\mathbf{s}_m),)$ placed at $\{\mathbf{s}_1, \mathbf{s}_2, \cdots, \mathbf{s}_m\}$. $\mathbf{A}$ is an $n \times m$ matrix, whose (i, j)-entry is given by

$$A_{ij} = -\frac{\mu_0}{4\pi} \frac{1}{|\mathbf{r}_i - \mathbf{s}_j|^3} \left[1 - \frac{3(\mathbf{r}_i - \mathbf{s}_j)_z^2}{|\mathbf{r}_i - \mathbf{s}_j|^2}\right], \tag{2}$$

where μ_0 is the vacuum permeability. Given knowledge about the field profile we want to correct, the configuration of the shim pieces can be obtained by solving Eq. (1) numerically.

Figure 1(a) shows a cryogen-free variable-field superconducting magnet (mCFM-7T-50-H3, Cryogenic Ltd.) used in this work. It has a bore with a diameter of

51 mm and is capable of producing a magnetic field of up to 7 T. The nominal field homogeneity over the spherical volume with a diameter of 10 mm at the magnet center is ca. 0.1% (i.e. 1000 ppm). In order to measure the actual field distribution, we made a microcoil with an inner diameter of 0.4 mm. The microcoil was tuned at 82 MHz and attached to a homebuilt non-magnetic xyz stage. For a magnet current of 20.5 A, we measured ^{1}H NMR signals of paraffin for 847 different coil positions. The field distribution determined from the peak positions is shown in Fig. 1(b). The x-, y- (radial), and z- (axial) dependence, plotted in Fig. 1(c), shows a field profile typical of that within a multilayered solenoid coil.

In order to confirm the feasibility of paramagnetic shimming over a wide range of magnetic fields, we focus in this work on axial field correction with a range of $-4.0 \leq z \leq 4.0$ mm. Extension to a larger region is straightforward. For this purpose, we built a probe equipped with a 10-mm-tall saddle coil, in which a capillary sample tube can be put along the probe axis. Figure 1(d) shows re-measured field distribution along the capillary axis, which seemed to be slightly tilted from the z-axis of the stage used to obtain the data in Fig. 1(b) and (c). We found that the original field profile B_{orig} was well approximated by a quadratic function of z as

$$B_{\mathrm{orig}}(z) = (1 - az^2)B_0 \quad \text{with} \quad a = 32.7 \times 10^{-6}\ \mathrm{mm}^{-2}. \tag{3}$$

Here, B_0 is the magnetic field at $z = 0$. Figure 1(e) shows a histogram representing the resonance frequency distribution, which indicates asymmetric line broadening over ca. 540 ppm due to the field inhomogeneity.

Now, we show that a pair of cylindrical paramagnetic pellets, placed as shown in Fig. 2, is effective for compensating this type of field inhomogeneity in a

region between the pellets. To calculate the shim field $B_{\rm shim}(z)$ at a position $(0,0,z)$ according to Eqs. (1) and (2), it is convenient to introduce a cylindrical coordinate system (r,ϕ,z'):

$$\begin{aligned} B_{\rm shim}(z) &= -\frac{\mu_0}{4\pi}\frac{\chi_{\rm v}B_0}{\mu_0}\int_0^R r{\rm d}r\int_0^{2\pi}{\rm d}\phi\left(\int_d^{d+t}{\rm d}z'+\int_{-d-t}^{-d}{\rm d}z'\right) \\ &\quad \left\{\left[r^2+(z-z')^2\right]^{-\frac{3}{2}}-3(z-z')^2\left[r^2+(z-z')^2\right]^{-\frac{5}{2}}\right\} \\ &= \frac{\chi_{\rm v}B_0}{2}R^2\left(\int_d^{d+t}{\rm d}z'+\int_{-d-t}^{-d}{\rm d}z'\right)\left[R^2+(z-z')^2\right]^{-\frac{3}{2}}, \end{aligned} \tag{4}$$

where $\chi_{\rm v}$ is the volume magnetic susceptibility of the paramagnetic material, from which the magnetization per unit volume μ is given by

$$\mu = \frac{\chi_{\rm v}B_0}{\mu_0}. \tag{5}$$

As described in Fig. 2, R and t are the radius and thickness of the pellet, and d represents the distance between the origin ($z=0$) and the inner face of the pellet. By the following substitution

$$\theta = \tan^{-1}\left(\frac{z-z'}{R}\right), \quad {\rm d}z' = -\frac{R{\rm d}\theta}{\cos^2\theta}, \tag{6}$$

we obtain from Eq. (4)

$$\begin{aligned} B_{\rm shim}(z) &= \frac{\chi_{\rm v}B_0}{2}\left\{\frac{z+d+t}{[R^2+(z+d+t)^2]^{1/2}}-\frac{z-d-t}{[R^2+(z-d-t)^2]^{1/2}}\right. \\ &\quad \left.-\frac{z+d}{[R^2+(z+d)^2]^{1/2}}+\frac{z-d}{[R^2+(z-d)^2]^{1/2}}\right\}. \end{aligned} \tag{7}$$

What we should do is to optimize the parameters R, d, t, and $\chi_{\rm v}$, so that the z-dependence of the sum $B_{\rm orig}+B_{\rm shim}$ is minimized. We expand Eq. (7) into a power series of $\zeta \equiv z/R$ as

$$B_{\rm shim} = \chi_{\rm v}\left[G_0+G_2\zeta^2+G_4\zeta^4+O(\zeta^6)\right]B_0, \tag{8}$$

where

$$G_0 = \frac{\delta+\tau}{[(\delta+\tau)^2+1]^{1/2}} - \frac{\delta}{(\delta^2+1)^{1/2}}, \tag{9}$$

$$G_2 = -\frac{3}{2}\left[\frac{\delta+\tau}{[(\delta+\tau)^2+1]^{5/2}} - \frac{\delta}{(\delta^2+1)^{5/2}}\right], \tag{10}$$

$$G_4 = \frac{5}{8}\left[\frac{(\delta+\tau)\,[4(\delta+\tau)^2-3]}{[(\delta+\tau)^2+1]^{9/2}} - \frac{\delta(4\delta^2-3)}{(\delta^2+1)^{9/2}}\right], \tag{11}$$

with

$$\delta \equiv \frac{d}{R}, \quad \tau \equiv \frac{t}{R}. \tag{12}$$

For convergence, $|\zeta|$ must be smaller than 1. In this work, we set R to 9.00 mm, so that $|\zeta|$ is at most ca. 0.44. Under the condition $\chi_{\rm v} G_2 = aR^2$ and $G_4 = 0$, we obtain $d = 8.63$ mm, $t = 6.30$ mm, and $\chi_{\rm v} = 0.0139$ (in SI unit). In Fig. 3 plotted are the calculated field profiles with and without the shim pieces with this configuration, showing significant improvement in the field homogeneity.

Since the susceptibility $\chi_{\rm v} = 0.0139$ that we now require is relatively large, candidate materials are insulating solids including transition metal ions or rare earth ions. The former have partially filled electronic d shells, while in the latter partially filled f shells come into play for the paramagnetism. Even though both are known to obey Curie's law, the rare earth ions show some preferable features. First, the effective Bohr magneton number is relatively large, so that field correction would be easier. Second, for the rare earth ions, the partially filled $4f$ shells lie beneath the filled $5s$ and $5p$ shells. As a result, the paramagnetism is not affected by crystal field splitting very much, and therefore is insensitive to the chemical environment. In general, agreement between the theoretical and measured effective Bohr magneton is excellent[7]. In contrast, for the transition metal ions, the $3d$ shells are the outmost electronic shells, and are strongly influenced by the crystalline environment, and thus by

the chemical composition and impurities. The low toxicity of the rare earth elements is also preferred.

We looked up various insulating solids containing rare earth ions[8], and estimated their volume susceptibilities from their compositions, densities, and the effective Bohr magneton numbers. Out of more than a hundred compounds, we selected dysprosium (III) oxide (Dy_2O_3), because of its large susceptibility, safety, and availability with moderate price. Experimental studies on the susceptibility of Dy_2O_3 are also found in literature[9,10].

3 Results and discussion

We prepared aqueous solution of a mixture of lithium, rubidium, and scandium chlorides with a mass ratio of $LiCl:RbCl:ScCl_3{\cdot}6H_2O:H_2O = 1:12:2:20$. The sample was doped with manganese (II) chloride to shorten spin–lattice relaxation times and was put into the capillary with an inner diameter of 1.0 mm. The sample length in the capillary was adjusted to 8.0 mm, and both ends of the capillary were sealed with epoxy glue. Variable-field measurements of ^{7}Li, ^{87}Rb, and ^{45}Sc NMR were performed at a constant carrier frequency of 56.0 MHz by using the Hahn echo sequence. Figure 4 shows ^{7}Li, ^{87}Rb, and ^{45}Sc spectra obtained at magnetic fields of 3.4, 4.0, and 5.4 T, respectively. The similar broad and asymmetric lineshapes of these three signals would be ascribable to the field distribution, as described in Fig. 1(e).

In order to compensate the field inhomogeneity, we fabricated paramagnetic shim pellets using Dy_2O_3 powder (Aldrich). The actual mass magnetic susceptibility of Dy_2O_3 was measured with a SQUID fluxmeter (MPMS-XL7ACMKO,

Quantum Design, Inc.) at 300 K to be 3.09 $mm^3\ g^{-1}$ in SI unit, and the proportionality of the magnetization to the applied field was verified throughout the range of 0–7 T, as shown in Fig. 5. The volume susceptibility χ_v of the paramagnetic shim pieces was adjusted by diluting Dy_2O_3 with KBr, whose susceptibility was measured to be negligible compared to that of Dy_2O_3. We mixed Dy_2O_3 and KBr with a mass ratio of 9.3:1 in an alumina mortar, and then the powder mixture was pressed into a pellet under 40 MPa using a stainless-steel mold. We made a pair of pellets with the optimized radius and height of 9.0 and 6.3 mm, respectively. The amount of Dy_2O_3 used for the two pellets was 13.5 g, which costed ca. 10,000 JPY. The volume magnetic susceptibility of each pellet was estimated to be 0.013 from the content of Dy_2O_3. These paramagnetic shim pieces, called the top and bottom shims henceforth, were attached above and below the capillary, as shown in Fig. 6. Their position d can be adjusted independently with a range of 5.0–11.4 mm.

We measured ^{45}Sc signals with varying positions of the top and bottom shim pieces. We started from $d = 5.0$ mm, and as increasing d for both pieces symmetrically, the resonance line became narrower. The minimum linewidth was obtained for $d = 7.1$ mm. Then, we adjusted the positions of the top and bottom shims independently and found that the resonance line was the narrowest for $d = 6.7$ and 7.2 mm, respectively. The optimal distance between the shim pellets was shorter than the predicted value ($d = 8.63$ mm). Keeping the shim pellets at the optimal position, we also measured the ^7Li and ^{87}Rb signals. As demonstrated in Fig. 6, similar lineshapes with full width at half maximums (FWHMs) of ca. 58 ppm were obtained. Moreover, the spectral distribution (ca. 100 ppm) was significantly reduced compared to that without the shim pellets.

To estimate the minimum possible linewidth, we measured the spin-spin relaxation times of the ^{7}Li, ^{87}Rb, and ^{45}Sc spins in the present sample with the Carr–Purcell–Meiboom–Gill method to be 25, 1.6, and 1.4 ms, respectively. Thus, the intrinsic linewidth should be 4 ppm at most. However, the observed FWHMs (ca. 58 ppm) were much larger than this. The residual field inhomogeneity would have arisen from several reasons. One may be discrepancy of the actual χ_{v} (0.013) from the intended value (0.0139). It presumably explains the result that the optimal d (6.7 and 7.2 mm) was smaller than the predicted value (8.63 mm).

When we made the paramagnetic shim pellets by diluting Dy_2O_3 with KBr, we assumed that the powders were uniformly mixed before being pressed. If, however, the uniformity was locally broken, an unexpected magnetic field may have developed. Accuracy in the geometry of the pellets as well as their position and alignment should also matter. For these reasons, we made the mobile shim pellets around the predicted optimal position, which enabled us to seek for the positions that minimize the measured linewidth. However, the displacement of the pellets from the calculated value should have lifted the fourth-order term in Eq. (11), causing another broadening effect. In fact, we calculated the field profile for the actual configuration and found that the field caused by the displacement of the pellets distributes over a range of 86 ppm, which is consistent with the experimental results.

For practical applications to NMR/MRI of larger volume samples, field correction along the radial direction would be required. From the x/y-dependence of the field in our magnet shown in Fig. 1(c), the radial field distribution can be well approximated by a concave quadratic function as $B(r) = (1+br^2)B_0$ with $b = 14.6 \times 10^{-6}$ mm^{-2}. For this type of field inhomogeneity, a paramagnetic

ring or *washer*, i.e., a thin disk-shaped plate with a hole in the middle, may be used. When the washer is placed with its axis being parallel to the z axis, the radial dependence of the magnetic field $B_{\mathrm{shim}}(r)$ produced inside the hole is given by

$$B_{\mathrm{shim}}(r) = -\frac{\mu_0}{4\pi}\frac{\chi_{\mathrm{v}}B_0}{\mu_0}t\int_{R_{\mathrm{i}}}^{R_{\mathrm{o}}} R\mathrm{d}R\int_0^{2\pi}\mathrm{d}\phi\left(R^2+r^2-2rR\cos\phi\right)^{-\frac{3}{2}}. \tag{13}$$

Here, R_{i}, R_{o}, and t are the inner radius, outer radius, and thickness of the washer, and we assume that $t \ll R_{\mathrm{i}}$. Integration over ϕ can be done by employing the complete elliptic integral of the second kind E as

$$B_{\mathrm{shim}}(r) = -\frac{\chi_{\mathrm{v}}B_0}{4\pi}t\int_{R_{\mathrm{i}}}^{R_{\mathrm{o}}}\mathrm{d}R\frac{4R}{(R+r)(R-r)^2}E\left(\frac{2\sqrt{rR}}{R+r}\right). \tag{14}$$

We now expand the integrand of Eq. (14) into a Taylor series, and then proceed with the integration. We finally obtain

$$B_{\mathrm{shim}}(r) = \chi_{\mathrm{v}}\left[F_0+F_2r^2+O(r^4)\right]B_0, \tag{15}$$

where

$$F_0 = -\frac{1}{2}t\left(R_{\mathrm{i}}^{-1}-R_{\mathrm{o}}^{-1}\right), \tag{16}$$

$$F_2 = -\frac{3}{8}t\left(R_{\mathrm{i}}^{-3}-R_{\mathrm{o}}^{-3}\right). \tag{17}$$

Thus, the paramagnetic washer is expected to work for radial field correction, if the dimension of the washer may be set so as to satisfy $\chi_{\mathrm{v}}F_2 = b$. If non-axial field correction along, say, the x direction, is necessary, the paramagnetic washer may be cut in half. One can verify that such a semicircle ring should work by replacing r of Eq. (13) by x and by restricting the range of integration over ϕ to $(-\pi/2, \pi/2)$. However, given that we already confirmed the idea of paramagnetic shimming through demonstration of axial field correction, that the quadratic field profile is only specific to the magnet that we used, and that the washer would induce additional axial field distribution, the development

and fine adjustment of the paramagnetic washer would add little new information regarding to our feasibility study of paramagnetic shimming over a wide range of magnetic fields. In practice, iterative numerical optimizations based on Eqs. (1) and (2) together with field-distribution measurements would be required. Importantly, such optimization is required only for one given field, as discussed above.

It should also be noted that the magnetic susceptibility depends on temperature. According to the Curie's law, the paramagnetic susceptibility is inversely proportional to temperature. The shim field $B_{\mathrm{shim}}(\mathbf{r};T)$ at temperature T is expressed as

$$B_{\mathrm{shim}}(\mathbf{r};T) = \frac{\alpha(\mathbf{r})}{T} B_0, \tag{18}$$

where $\alpha(\mathbf{r})$ is a function of $\mathbf{r}$. B_{shim} changes with temperature variation ΔT by

$$\begin{aligned} B_{\mathrm{shim}}(\mathbf{r};T+\Delta T) - B_{\mathrm{shim}}(\mathbf{r};T) &= -\frac{\alpha(\mathbf{r})\Delta T}{T(T+\Delta T)} B_0 \\ &= -\frac{\Delta T}{T+\Delta T} B_{\mathrm{shim}}(\mathbf{r};T). \end{aligned} \tag{19}$$

In our present case, since B_{shim} is approximately given by $\chi_{\mathrm{v}} G_0 + az^2$, the difference is calculated to be at most ca. 10 ppm per Kelvin at room temperature. Therefore, the temperature effect was expected to be small compared to the observed linewidths. For finer shimming, however, a temperature regulator will be required.

As increasing the magnetic field or decreasing the temperature, the paramagnetic magnetization saturates eventually. The extent to which the Dy_2O_3 paramagnetic pellets used in this work exhibit linear behavior can be estimated from the condition $\tanh(\mu_{\mathrm{B}}^{\mathrm{eff}} B_0 / k_{\mathrm{B}} T) \ll 1$. If we assume that $\mu_{\mathrm{B}}^{\mathrm{eff}} \sim 10\mu_{\mathrm{B}}$ and

require $(\mu_{\mathrm{B}}^{\mathrm{eff}} B_0/k_{\mathrm{B}}T)^2/3 < 10^{-2}$, the linearity is assured at room temperature up to 7.7 T, well above the magnetic field used in the present study. When paramagnetic shimming is to be applied to higher magnetic fields, paramagnetic materials involving rare earth ions with smaller effective Bohr magneton numbers may be the choice.

To summarize, we demonstrated the applicability of paramagnetic shimming to variable-field NMR experiments. Owing to the paramagnetism of the shim pieces, the multi-nuclear spectra obtained at different magnetic fields were equally narrowed with a common shim configuration. Paramagnetic shimming we presented in this work opens a way toward high-resolution variable-field NMR experiments. Possible applications include high-resolution NMR elemental analysis and quantitative multi-nuclear MRI, which are planned and will be reported elsewhere.

Acknowledgements

This work was supported by Grant-in-Aid for Challenging Exploratory Research (No. 24655010) of Japan Society for the Promotion of Science (JSPS). The SQUID measurements were carried out using facilities of Research Center for Low Temperature and Materials Sciences, Kyoto University. We thank K. Izawa, S. Satake, M. Sugimoto, and T. Takasaki for helping elaborate field-distribution measurements.

References

[1] W. A. Anderson, Electrical Current Shims for Correcting Magnetic Fields, Rev. Sci. Instrum., 32 (1961) 241–250.

[2] D. I. Hoult, D. Lee, Shimming a superconducting nuclear-magnetic-resonance imaging magnet with steel, Rev. Sci. Instrum., 56 (1985) 131–135.

[3] K. Takeda, N. Ichijo, Y. Noda, K. Takegoshi, Elemental analysis by NMR, J. Magn. Reson., 224 (2012) 48–52.

[4] K. M. Koch, P. B. Brown, D. L. Rothman, R. A. de Graaf, Sample-specific diamagnetic and paramagnetic passive shimming, J. Magn. Reson., 182 (2006) 66–74.

[5] C. Juchem, B. Muller-Bierl, F. Schick, N. K. Logothetis, J. Pfeuffer, Combined passive and active shimming for in vivo MR spectroscopy at high magnetic fields, J. Magn. Reson., 183 (2006) 278–289.

[6] L. Hong, D. Zu, Shimming Permanent Magnet of MRI Scanner, PIERS Online, 3 (2007) 859–864.

[7] N.W. Ashcroft, N.D. Mermin, Solid State Physics, International Edition, Saunders College (1976).

[8] CRC Handbook of Chemistry and Physics, 92th Edition, Taylor & Francis.

[9] S. Arajs, R. V. Colvin, Magnetic Susceptibility of Gadolinium and Dysprosium Sesquioxides at Elevated Temperatures, J. Appl. Phys., 33 (1962) 2517–2519.

[10] Y. Gossuin, A. Hocq, Q. L. Vuong, S. Disch, R. P. Hermann, P. Gillis, Physico-chemical and NMR relaxometric characterization of gadolinium hydroxide and dysprosium oxide nanoparticles, Nanotechnology, 19 (2008) 475102.

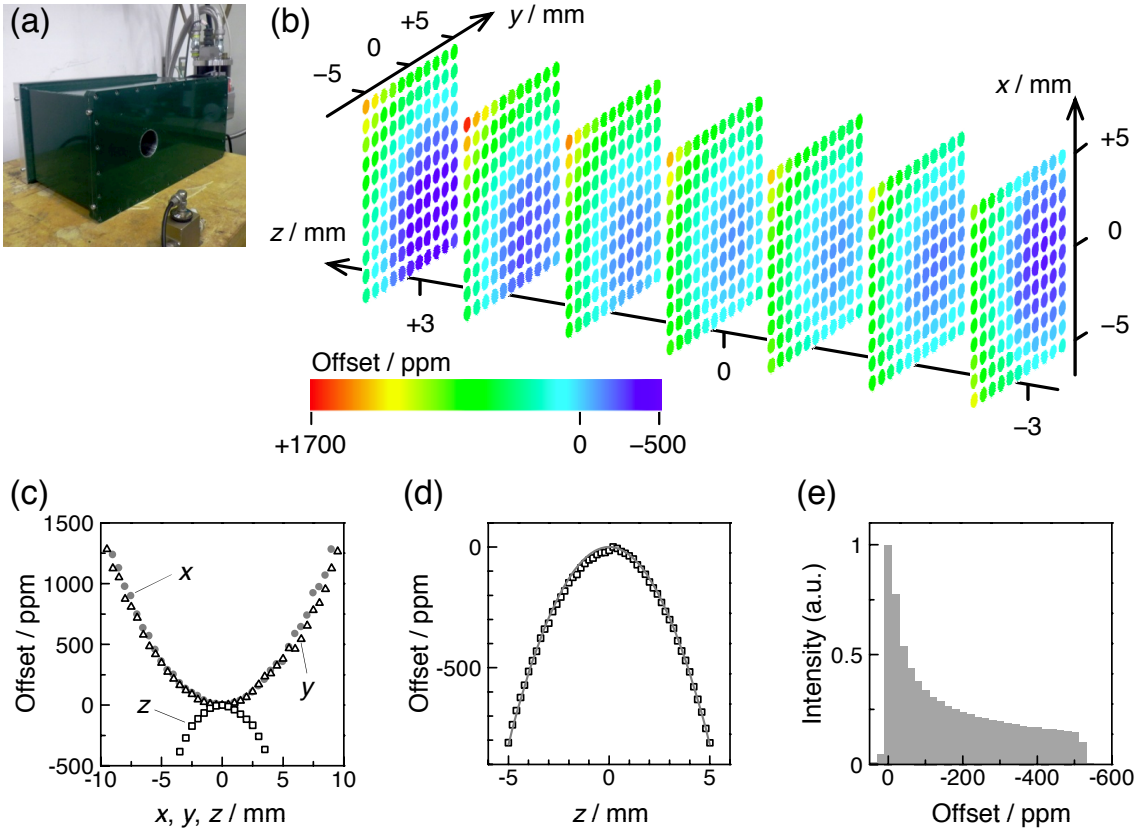

Fig. 1. (a) A snapshot of a cryogen-free superconducting magnet (mCFM-7T-50-H3, Cryogenic Ltd.). (b) Measured field distribution determined from the ^{1}H resonance frequency of paraffin in a microcoil with an inner diameter of 0.4 mm. Measurements were performed over 847 positions of the microcoil with x- and y-intervals of 0.5 mm and a z-interval of 1 mm. The carrier frequency was 82 MHz and the magnet current was 20.5 A. x-, y-, and z-dependences of the magnetic field are plotted in (c) with circles, triangles, and squares, respectively. (d) Field distribution along the capillary sample tube. Using a microcoil with a coil diameter of 0.1 mm, ^{1}H NMR signals of glycerol were measured for various positions by sliding the microcoil inside the empty capillary. The solid line is a fitted curve of the experimental data (squares) using a quadratic function (see Eq. (3)). The magnet current was set to 36.1 A, and the carrier frequency was 56.0 MHz. (e) A histogram of resonance frequency distribution over a range of $-4 \leq z \leq 4$ mm.

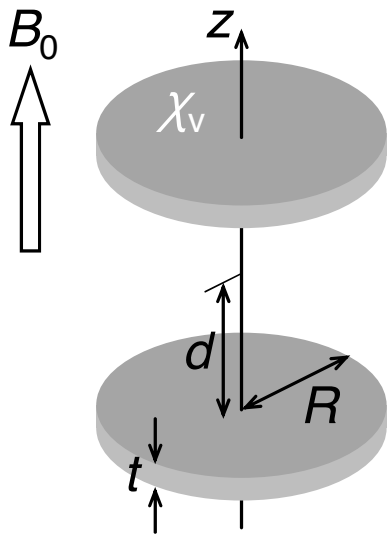

Fig. 2. A configuration of a pair of paramagnetic shim pellets with a radius R and a thickness t. d is the distance between the inner face of the pellets and the origin ($z = 0$). χ_{v} represents the volume magnetic susceptibility.

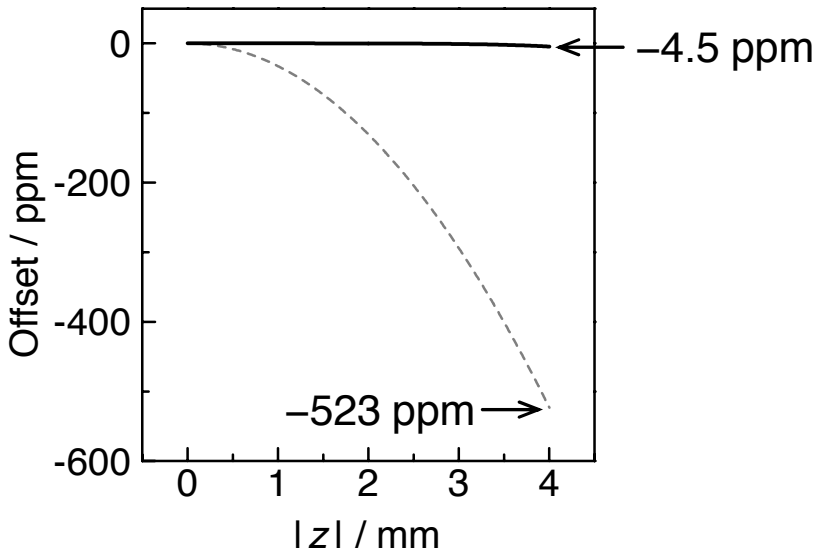

Fig. 3. Calculated field profiles with (solid line) and without (broken line) the shim pellets for $R = 9.00$ mm, $d = 8.63$ mm, $t = 6.30$ mm, and $\chi_{\mathrm{v}} = 0.0139$.

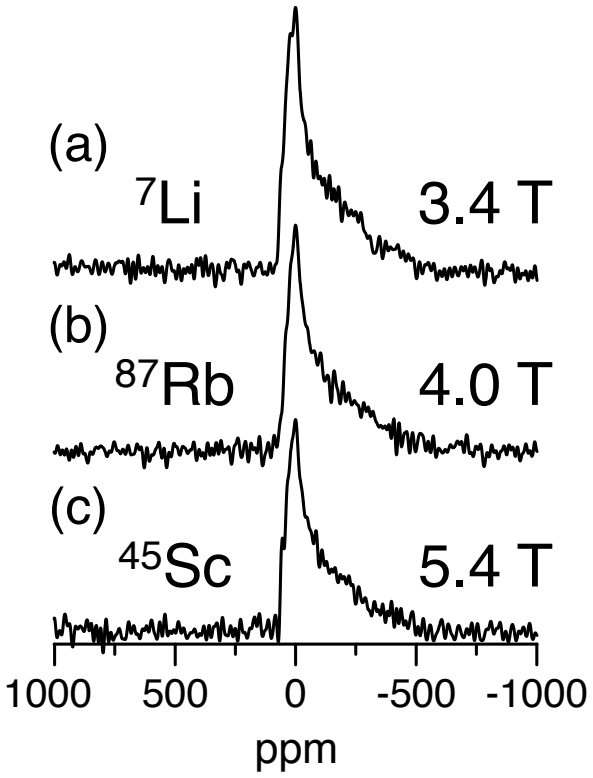

Fig. 4. NMR spectra of (a) ^{7}Li, (b) ^{87}Rb, and (c) ^{45}Sc nuclei in aqueous solution of a mixture of LiCl, RbCl, and $ScCl_3$ measured in magnetic fields of 3.4, 4.0, and 5.4 T, respectively. No shimming was performed.

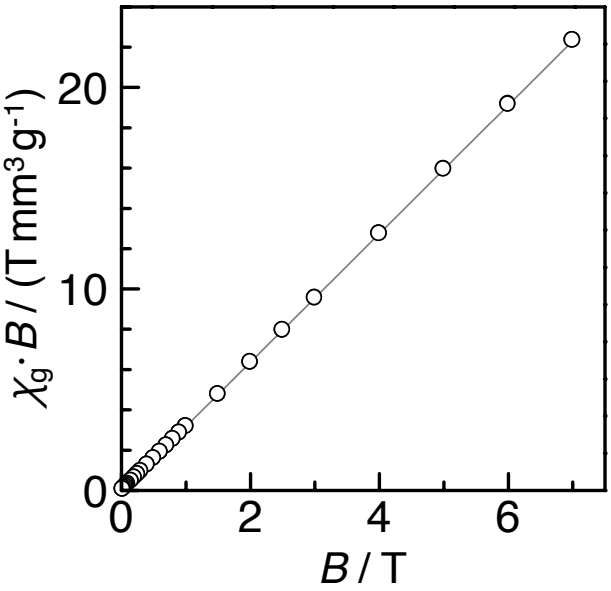

Fig. 5. A result of SQUID measurements of Dy_2O_3 showing field (B) dependence of the magnetic flux. The mass susceptibility χ_g is given by the slope of the solid line obtained by least-square fitting to be 3.09 mm^3g^{-1}. The coefficient of determination was 0.99999513 (1-4.87×10^{-6})

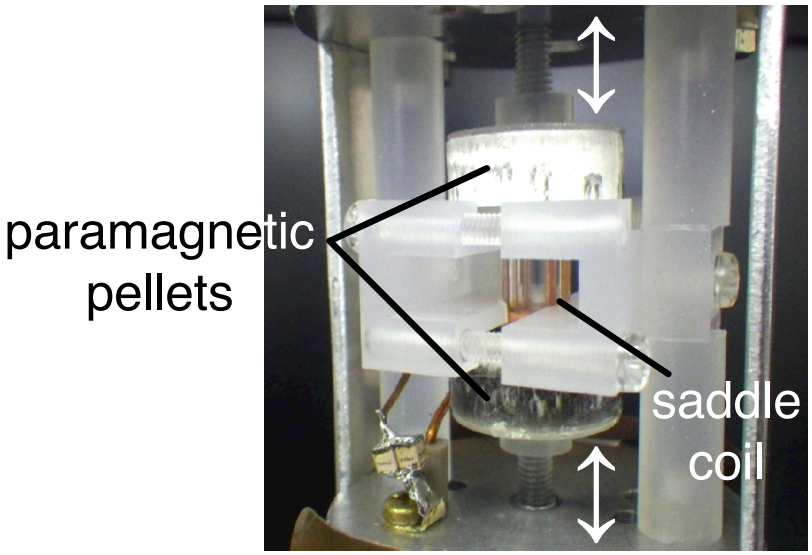

Fig. 6. A snapshot of the probehead composed of a tuned saddle coil and a pair of paramagnetic pellets. Their vertical positions can be adjusted independently.

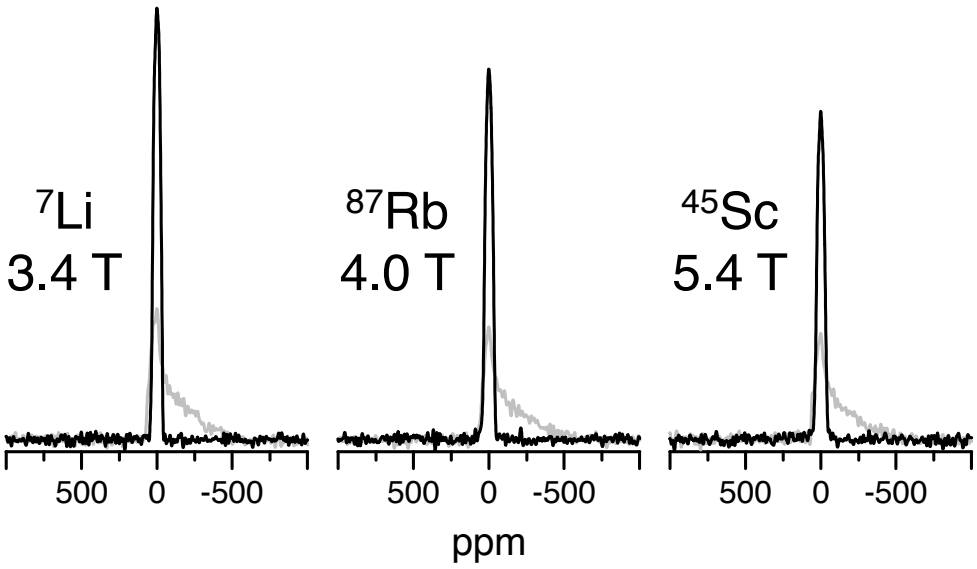

Fig. 7. ^{7}Li, ^{87}Rb, and ^{45}Sc spectra obtained using the paramagnetic shim pellets with the optimized configuration. For comparison, the spectra obtained without shimming are shown in the gray lines. The number of scans was 8000 for each spectrum.